JET PROPULSION LABORATORY
CALIFORNIA INSTITUTE OF TECHNOLOGY
PASADENA, CALIFORNIA

NATIONAL AERONAUTICS AND SPACE ADMINISTRATION
CONTRACT NO. NASw-6

Technical Release No. 34-146

TRAJECTORIES AND THRUST-MEASUREMENT TECHNIQUES FOR SPACE TESTING OF ION ROCKET MOTORS

David G. Elliott

JET PROPULSION LABORATORY
A RESEARCH FACILITY OF
NATIONAL AERONAUTICS
AND SPACE ADMINISTRATION
OPERATED BY
CALIFORNIA INSTITUTE OF TECHNOLOGY
PASADENA, CALIFORNIA
November 1, 1960

CONTENTS

FIGURES

FIGURES (Cont'd)

TRAJECTORIES AND THRUST-MEASUREMENT TECHNIQUES FOR SPACE TESTING OF ION ROCKET MOTORS[1,2]

David G. Elliott[3]

Jet Propulsion Laboratory
California Institute of Technology
Pasadena, California

ABSTRACT

In laboratory tests of ion rocket motors the presence of vacuum-chamber walls and residual gas can greatly influence the behavior of the ion-motor exhaust. Hence, final proof of the feasibility of ion motors will probably require actual space tests. The problems of conducting such a space test are discussed from the standpoint of power supplies, attainable thrusts and test durations, suitable trajectories, and thrust-measurement techniques. The simplest thrust-measurement technique is found to be measurement of changes in angular motion. The equations of motion for a body under the influence of a small torque are solved to give the angular motion of an ion-motor test vehicle and show the effects of vehicle configuration. Numerical results are given for attainable angular accelerations, total angular velocity changes, centrifugal forces on the ion motor, and exhaust curvature. The magnitudes of extraneous torques due to the Earth's magnetic field and to vehicle elasticity are discussed. Several methods of measuring the angular acceleration produced by the ion motor are presented. An example is given of a specific ion-motor test vehicle employing an ion motor of 10-mlb thrust and launched by a Scout.

---

[1]This paper presents the results of one phase of research carried out at the Jet Propulsion Laboratory, California Institute of Technology, under Contract No. NASw-6, sponsored by the National Aeronautics and Space Administration.

[2]Presented at the ARS Electrostatic Propulsion Conference, U.S. Naval Postgraduate School, Monterey, California, November 3-4, 1960.

[3]Engineering Group Supervisor. Member ARS.

ELECTROSTATIC PROPULSION

INTRODUCTION

Unlike other types of rocket motors, the ion motor depends for its operation on the behavior of the exhaust downstream of the motor. Electrostatic forces can arise between the exhaust and the vehicle, so that the thrust is not equal to the momentum flux of the exhaust at the motor exit. At the present time no certain method has been found for calculating these electrostatic forces or duplicating them in ground test facilities. Hence, there is widespread interest in testing ion motors in space to determine if the electrostatic space-charge of the exhaust can be adequately neutralized and to compare the thrust in space with that measured in the laboratory. Such a test would also provide information on the engineering problems of operating ion motors in flight and on problems of communicating through the exhaust.

The design of an ion-propelled vehicle for performing ion-motor space tests is discussed from the standpoint of power supplies, attainable thrusts and test durations, suitable trajectories, and thrust-measurement techniques. The emphasis is on minimal tests for basic verification of ion-motor performance.

THRUST AND TEST DURATION

The thrust levels of interest for an early ion-motor space test range from about 1 mlb (1 millipound = 0.001 lb_f) to 10 mlb. With thrusts below 1 mlb the ratio of beam diameter to acceleration distance may be small enough to yield a thrust even with little or no space-charge neutralization, in which case the results would be invalid for practical ion motors. With higher thrusts a meaningful space test is more nearly assured. However, the largest ion motors currently under development, at least of the cesium contact ionization type, are of about 10-mlb thrust, setting this level as the approximate upper limit for early space tests.

The durations of interest for early ion-motor space tests range from a few minutes to several days. With several minutes' test time above the atmosphere it might be possible to start an ion motor and quickly measure its thrust. With hours or days in space highly accurate thrust measurements, and variations of motor operating conditions, are possible. Durations beyond several days require solar or nuclear power sources, an unnecessary complication for early ion-motor performance tests.

ELECTROSTATIC PROPULSION

For the thrusts and test durations of interest, the simplest and lightest power source is a battery and inverter. The allowable thrusts and test durations are then related, through the power-supply weight, to the weight which can be launched into the desired trajectory.

Battery Energy and Weight

The lightest type of battery for a given energy in watt-hours is the silver oxide–zinc manually activated primary battery; manually activated in that the electrolyte is added by hand before use, and primary in that no, or at most a few, recharges are possible.

The silver-zinc battery consists of oxidized silver cathodes separated from porous zinc anodes by cellulose separators. When the potassium hydroxide electrolyte is added it is absorbed by the separators. A single cell has a nominal operating voltage of 1.5v, and large batteries are customarily connected for 28v. In such a battery the cells are contained in a magnesium or stainless-steel case which can be exposed directly to vacuum since the case is sealed except for relief vents which can open to prevent buildup of excessive internal pressure.

For currents corresponding to discharge times of an hour or longer the output voltage remains nearly constant until the battery is almost completely discharged, then drops rapidly to zero. For such discharge times the energy delivered is about 55 whr per lb of battery weight, including the case and mounting hardware (Ref. 1). Thus, the weight of the battery can be written

$$M_b = \frac{P_b t}{0.055} \qquad (1)$$

where P_b is the power output of the battery in kilowatts and t is the test duration in hours.

Inverter Power and Weight

To supply the high dc voltages required for operating the ion motor an inverter is required. An inverter employs transistor switching to convert the 28-v dc battery output to 28-v ac, typically square wave at 2400 cps. A transformer with multiple secondary windings, feeding silicon rectifiers and filters, provides the accelerating and decelerating voltages for the ion motor as well as the voltages for the telemetry equipment.

Fig. 1 presents the approximate weight of inverters as a function of the output power. It is seen that for 2-kw output power, as approximately required for an ion motor of 10-mlb thrust, the inverter weighs about 21 lb_m.

Inverters have an efficiency of about 85%, 15% of the input power being dissipated as heat. Thus, the inverter output power is

$$P_i = 0.85\ P_{bi} \qquad (2)$$

where P_{bi} is the portion of the battery power supplied to the inverter.

The alternative to an inverter is a large number of battery cells in series. However, the large number of cells and the additional insulation between cells would add more weight than the inverter.

Telemetry Capability and Weight

Telemetry is needed on an ion-motor space test to confirm that the ion motor is operating and to provide values of the operating voltages, currents, and temperatures for correlation with the thrust and comparison with previous laboratory measurements. Except for possible high-frequency oscillations, these data require relatively low bandwidth, and a standard IRIG FM/FM telemetry system can be used. This system provides 16 simultaneous channels ranging in bandwidth from 6 to 600 cps, with the option of commutating one or more channels to accommodate larger numbers of parameters.

The weight of such a telemetry system, including a 10-w transmitter and antenna, is 20 lb_m or less, assuming the power is supplied from the main inverter. The power required for the telemetry and miscellaneous control functions is conservatively estimated as 100 w.

Ion-Motor Thrust and Weight

Cesium-ion motors currently under development will achieve power efficiencies (exhaust-power/input-power) of 60% at specific impulses of about 6000 lb_f sec/lb_m. These figures will be assumed to hold for an ion-motor flight test. In addition, it will be assumed that the power used for the ion-emitter heater (40% of the total) can be supplied at low voltage directly from the battery. Thus, the power output required from the inverter is

$$P_i = 0.60\ P_m + P_t \qquad (3)$$

where P_m is the total input power to the ion motor and P_t is the power required by the telemetry.

For a specific impulse of 6000 lb_f sec/lb_m and a power efficiency of 60%, each millipound of thrust requires 0.22 kw total input power to the ion motor. Thus, the motor input power in kilowatts is

$$P_m = 0.22\ F \qquad (4)$$

where F is the thrust in millipounds.

A reasonable estimate of the weight of a small cesium-ion motor, including cesium supply system and valve, is about 6 lb_m for a motor of 1-mlb thrust, increasing by about 1 lb_m for each additional millipound of thrust. Thus, the weight of the ion motor is

$$M_m = 5.0 + F \qquad (5)$$

Vehicle Weight and Test Duration

The complete ion-motor test vehicle consists of the battery, inverter, ion motor, telemetry equipment, mechanical structure, and interconnecting electrical wiring. The weight of the structure, wiring, and miscellaneous items will be assumed to be 20% of the weight of the other components. Hence, the total vehicle weight is 1.2 times the sum of the battery weight from Eq. 1, the inverter weight from Fig. 1, the ion-motor weight from Eq. 5, and the telemetry weight of 20 lb_m.

Fig. 2 presents the ion-motor vehicle weight as a function of test duration for ion-motor thrusts of 2, 5 and 10 mlb. For 2-mlb thrust the vehicle weight ranges from 55 lb_m at 1-hr duration to 305 lb_m at 20-hr duration. For 5-mlb thrust the weight ranges from 80 lb_m at 1-hr duration to 635 lb_m at 20-hr duration, and for 10-mlb thrust the weight ranges from 120 lb_m at 1 hr to 1180 lb_m at 20 hr.

LAUNCH VEHICLES AND TRAJECTORIES

The launch vehicles to be employed by NASA in the near future are Scout, Thor-Agena B, Atlas-Agena B, and Atlas-Centaur. The Scout, shown in Fig. 3, is a relatively

inexpensive four-stage solid-propellant rocket which can place a payload of 150 lb_m in a 300-n. mi circular orbit. The other vehicles can orbit larger payloads than any shown in Fig. 2.

Two types of trajectories are of interest for ion-motor space tests: (1) an orbit and (2) a high-altitude probe trajectory. The orbit provides unlimited flight time but does not, in general, permit continuous tracking and data reception. The probe trajectory permits continuous data reception but is limited in flight time.

Scout Payload Capability for Ion-Motor Space Tests

Fig. 4 shows the capability of the Scout for launching an ion-motor test vehicle. The permissible ion-motor test-vehicle weight is shown as a function of the time spent above 250 n. mi as approximated, to within a few minutes, by the zero "g" flight times presented in Ref. 2. For a 300-n. mi circular orbit the payload is 150 lb_m and the flight time unlimited. For a probe trajectory the payload capability varies from 50 lb_m for 4-hr flight duration to 185 lb_m for 1-hr flight duration. The launch angle for the probe trajectory is 80 deg, which gives slightly longer flight times than a more nearly vertical trajectory, but requires downrange tracking for the latter portion of the flight.

Superimposed on Fig. 4 are portions of the curves from Fig. 2 showing the required ion-motor test-vehicle weight as a function of the test time. It is seen that an orbital trajectory permits testing a 2-mlb ion motor for 8 hr, a 5-mlb motor for 3.4 hr, and a 10-mlb motor for 1.5 hr. A probe trajectory permits testing the same motors for 2.5, 1.8, and 1.4 hr respectively.

THRUST-MEASUREMENT TECHNIQUES

The key parameter to be measured in an ion-motor space test is the thrust. Some of the thrust-measurement methods used in ground testing can also be applied to space tests. A sensitive strain gage can be employed in the motor mount, for example, with the output telemetered to the ground.

The most sensitive and meaningful thrust measurements, however, are those involving changes of the vehicle's motion. The thrust can change the motion in two ways: (1) linear acceleration of the center of mass of the vehicle and (2) angular acceleration of the vehicle about the center of the mass. The latter will be referred to as a spin test.

The linear-acceleration test requires stabilization of the thrust direction by motor gimballing, gas jets, or spinning of the vehicle. The spin test avoids these requirements.

The thrust of an ion rocket motor can be considered to consist of two parts: (1) the thrust due to the momentum flux of material leaving the motor and (2) the thrust due to electrostatic forces between the motor (or vehicle) and the exhaust. Thus, the thrust of the ion motor can be written

$$F = \dot{m}\, c - F_e \tag{6}$$

where $\dot{m}$ is the propellant flow rate, c is the exhaust velocity at a plane downstream of the last grid of the ion motor, and F_e is the electrostatic attraction between the vehicle and the exhaust downstream of that plane.

In a linear-acceleration test the ion-motor thrust F is determined from the vehicle acceleration by the relation

$$F = M \frac{dv}{dt} \tag{7}$$

where M is the mass of the vehicle and v is its velocity.

In a spin test the ion motor is mounted with its thrust line at a known distance D from the center of mass of the vehicle, and the thrust is determined from the rate of change of angular momentum L by the relation

$$F = \frac{1}{D} \frac{dL}{dt} \tag{8}$$

If the electrostatic force F_e does not act in the same direction as the momentum flux $\dot{m}c$, then the two quantities in Eq. 6 must be added vectorially. Such a situation would arise if the exhaust were attracted to one side by an electrostatic charge on the vehicle structure. It is important to prevent, or at least detect, any such deflection. In a linear-acceleration test the vehicle stabilization could be impaired and no net acceleration of the center of mass achieved. In a spin test the moment arm D would be altered, invalidating the thrust measurements.

Linear Acceleration Tests

If an ion-motor test vehicle were accelerated from rest in free space, the maximum velocity increment achieved for any combination of thrust, vehicle mass, and thrust duration

shown in Fig. 2 would be only 20 ft/sec (at 10-mlb thrust for 20 hr). The maximum free-space velocity increment for a vehicle launched by the Scout would be only 12 ft/sec (2-mlb thrust for 8 hr).

These velocity increments can be utilized in one of two ways: (1) to change the shape of the orbit if an orbital trajectory is used or (2) to produce a relative separation between the vehicle and an inertial reference object.

Orbital Changes

Fig. 5 shows two possible thrust programs for changing an initially circular orbit. Thrust program (a) employs tangential thrust and requires guidance of the vehicle. Thrust program (b) employs unidirectional thrust and permits spin stabilization of the vehicle.

The effect of the tangential thrust program is to raise the orbital altitude while the orbit remains substantially circular (for thrust durations of several hours or more). With a 20-ft/sec velocity increment and a 300-n. mi initial altitude, the orbit is raised by about 5.8 n. mi.

The effect of the unidirectional thrust program is to change the eccentricity of the orbit. For a 20-ft/sec velocity increment the apogee is raised, and the perigee lowered, by about 4.3 n. mi.

The most accurate standard tracking technique is two-way Doppler, which requires equipment weighing 20-30 lb_m in the vehicle. With Doppler tracking the apogee can be determined to within approximately ± 1.0 n. mi after two passes over the tracking station. This accuracy and time span are not adequate for measuring thrust when changes in motor operating conditions are made during the flight. However, the orbit can be precisely determined before and after the ion-motor test, yielding an accurate average value for the thrust during the test.

Motion Relative to a Reference Object

Another method for measuring the thrust of the ion motor, employing linear acceleration, is to separate a reference object from the vehicle and observe its motion relative to the vehicle. The reference object need not be external to the vehicle but could be a small weight released within the vehicle with its motion observed by photocells. Suppose, for example, that the

thrust is 10 mlb and the vehicle weight 200 lb_m, giving an acceleration of 5×10^{-5} g's. If the reference object can be separated with zero velocity relative to the center of mass of the vehicle, the separation distance after 1 sec will be 0.01 in., and the separation distance after 30 sec will be 9.0 in. Suppose, however, that the vehicle is rotating at 1.0 rpm, a rate unlikely to be improved upon without elaborate stabilization, and that the reference object is dropped 1 in. from the center of mass of the vehicle. The initial velocity of the reference object will carry it 0.1 in. relative to the center of mass in 1 sec and 3.0 in. in 30 sec, amounts which could mask the vehicle acceleration. Thus, the requirements for this thrust-measurement technique are to provide either good vehicle stabilization or a separation point very close to the center of mass, together with a relatively long path for the reference object with several position-measuring stages, or continuous measurement, to separate out the initial velocity. If these requirements can be achieved, however, the reference-object method provides a thrust measurement within a minute or less, permitting variation of test conditions during the flight.

Angular Acceleration Tests

Use of the ion motor to rotate the test vehicle circumvents the stabilization problems of the linear-acceleration test and produces a more readily observable type of motion change. Furthermore, the rate of rotation, being a frequency, permits simple and precise measurement techniques.

Fig. 6 shows a possible configuration for a spin-test vehicle. The vehicle employs a 10-mlb ion motor and fits within a permissible Scout payload envelope of 23-in. diameter by 31-in. length. From Fig. 4 the test duration for a 10-mlb ion motor on a high-altitude probe-type trajectory, employing the Scout, is 1.4 hr. To permit immediate start of thrust after attaining altitude, the ion-motor exit could be covered to permit evacuation and outgassing on the ground, with the cover jettisoned at high altitude.

From Eq. 4 the total input power to the ion motor is 2.20 kw, of which 60%, or 1.32 kw, is supplied by the inverter and 0.88 kw is supplied directly from the battery. With 0.1 kw drawn by the telemetry, the inverter output power is 1.42 kw, and the corresponding inverter weight from Fig. 1 is 19 lb.

From Eq. 5 the ion-motor weight is 15 lb_m. The inverter input power is 1.42/0.85 = 1.67 kw, giving a total battery output power of 1.67 + 0.88 = 2.55 kw. The required battery energy is therefore 2.55 × 1.4 = 3.57 kw-hr, and the battery weight from Eq. 1 is 3.57/0.055 = 65 lb_m. The telemetry weight is 20 lb_m. The sum of the inverter, battery, ion motor, and telemetry weights is therefore 119 lb_m. Adding 119 × 0.2 = 24 lb_m for structure, the total vehicle weight is 143 lb_m. Although there are numerous uncertainties in this weight estimate, it should be noted from Fig. 4 that the addition of even 100 lb_m would only reduce the flight time to 50 min.

For a 1.4-hr test with a 10-mlb ion motor, the propellant consumption is only 4 grams.

In the vehicle configuration shown in Fig. 6 the ion motor, assumed to be a cylinder 11 in. in diameter by 5 in. long, is mounted tangent to the axis of rotation. The battery, in a 12 × 14 × 7-in. case, is mounted below the ion motor. The inverter, telemetry equipment, and miscellaneous items are mounted in a 12 × 14 × 5-in. box above the ion motor. A trusswork structure connects the three parts.

The 1-, 2-, and 3-axes shown in Fig. 6 are the principal axes of the vehicle. Assuming for simplicity that the weights are distributed uniformly, with half the structural weight assigned to the battery and half to the telemetry and inverter box, it can readily be verified that the center of mass is at the origin of the 1-, 2-, and 3-axes and that the moments of inertia about these axes are

$$I_1 = I_2 = 56.6 \text{ lb}_f \text{ in. sec}^2$$
$$I_3 = 11.1 \text{ lb}_f \text{ in. sec}^2.$$

The center of the ion motor is at D = 5.5 in. from the center of mass of the vehicle, and the motor is oriented to produce a torque about the 3-axis only. The torque is DF = 0.055 lb_f in. and the resulting angular acceleration is

$$\frac{d\omega_3}{dt} = \frac{DF}{I_3} = 2.8 \text{ rpm/min}$$

Thus, during a 1.4-hr test a total spin-rate change of 235 rpm can be produced. Since the Scout fourth stage is spin-stabilized at 160 rpm, the ion-motor thrust can despin the vehicle from 160 rpm to 0 rpm and back to 75 rpm in the opposite direction.

Because of the continuing angular acceleration, zero-gravity conditions are not reached as the spin rate goes through zero, possibly obviating the need for a zero-gravity cesium feed system. The lowest acceleration reached at the center of the motor is 7×10^{-5} g's, which may be sufficient for operating a liquid cesium boiler. During most of the test the cesium is subjected to a much greater acceleration due to the spin of the vehicle. At the maximum spin rate of 160 rpm the centrifugal acceleration is 8 g's at the outer edge of the ion motor and 4 g's at the center. The motor must be strong enough to withstand these accelerations as well as the 16 g's attained during launch, although in the latter case the motor need not be hot.

The spin rate can be measured by various methods, to be discussed later, which yield an output varying at a frequency related to the spin frequency ω_3. The number of cycles of such data in a given time can typically be determined to within 0.2 cycles. Thus, observation of the spin frequency for 1 min gives a value with an uncertainty of about 0.2 rpm. If a second observation is made 10 min later, the maximum uncertainty in the frequency difference is 0.4 rpm, which is 1.4% of the 28-rpm frequency change during that time. Hence, the ion-motor thrust can be determined to within about 1.4% from 10 min of data, and probably from even less when more sophisticated data-reduction procedures are employed. Therefore, several changes in motor operating conditions could be made even during a 1.4-hr test.

As a result of the rotation of the ion motor the exhaust follows a spiral, rather than a straight path in space. However, even at 160 rpm the radius of curvature of the exhaust path is 2.2 mi, which does not appear small enough to affect the behavior of the ion motor appreciably.

When the ion-motor test vehicle is separated from the launch vehicle it will not be rotating exactly around the 3-axis, because of misalignment and separation forces. The resulting precession will complicate the spin-rate measurements and cause extraneous torques due to structural deflections. In addition, extraneous torques can be caused by the Earth's magnetic field. These detailed problems of an ion-motor space test will be considered in the remainder of the paper.

SPIN DYNAMICS OF ION-MOTOR VEHICLES

Fig. 7 shows the coordinate system for describing the motion of the ion-motor test vehicle. The x-, y-, and z-axes have their origin at the center of mass of the vehicle

and are fixed in space. The 1-, 2-, and 3-axes have their origin at the center of mass, are principal axes, and are fixed in the vehicle, with the 1-axis drawn through the ion motor. The moments of inertia about the 1-, 2-, and 3-axes are I_1, I_2, and I_3, respectively, and the body is symmetrical about the 3-axis; that is, $I_1 = I_2$. The angular velocities about the 1-, 2-, and 3-axes are ω_1, ω_2, and ω_3, respectively. The ion motor exerts a torque DF about the 3-axis and zero torque about the 1- and 2-axes. It will be assumed for the present that the vehicle is perfectly rigid. The effects of departures from these ideal conditions are described later.

Motion Relative to Vehicle Coordinates

The motion of the vehicle relative to the vehicle-fixed 1-, 2-, and 3-axes is described by Euler's equations, derived in numerous mechanics texts (e.g., Ref. 3). For $I_1 = I_2$ and zero torque about the 1- and 2-axes, Euler's equations are

$$\dot{\omega}_1 - \left(1 - \frac{I_3}{I_1}\right)\omega_3\,\omega_2 = 0 \tag{9}$$

$$\dot{\omega}_2 + \left(1 - \frac{I_3}{I_1}\right)\omega_3\,\omega_1 = 0 \tag{10}$$

$$\dot{\omega}_3 = \frac{DF}{I_3} \tag{11}$$

where the dot over a symbol denotes differentiation with respect to time.

The solution of these equations is

$$\omega_1 = \omega_p \sin\left[\frac{1}{2}\left(1 - \frac{I_3}{I_1}\right)(\omega_3 + \omega_0)\,t + \text{const}\right] \tag{12}$$

$$\omega_2 = \omega_p \cos\left[\frac{1}{2}\left(1 - \frac{I_3}{I_1}\right)(\omega_3 + \omega_0)\,t + \text{const}\right] \tag{13}$$

$$\omega_3 = \frac{DF}{I_3}\,t + \omega_0 \tag{14}$$

where t is the time measured from the instant the ion motor is turned on and ω_0 and ω_p are the initial angular velocities about the 3-axis and perpendicular to the 3-axis, respectively. The angular velocity ω_0 is the initial spin rate imparted to the vehicle, and ω_p is the angular velocity imparted perpendicular to the spin axis by errors in alignment and by vehicle separation forces.

According to Eq. 14 the spin rate ω_3 increases linearly with time at a rate DF/I_3. If the vehicle is de-spun, F is considered to be negative. Eq. 14 also shows that the spin rate ω_3 is unaffected by the motion about the 1- and 2-axes, and, in particular, is independent of ω_p. It is to obtain a steady angular acceleration, dependent only on thrust, that I_1 is made equal to I_2. The effect of having these moments of inertia unequal is discussed later.

Squaring and adding Eq. 12 and 13 shows that

$$\omega_1^2 + \omega_2^2 = \omega_p^2 \tag{15}$$

Thus, the magnitude of the angular velocity perpendicular to the 3-axis remains constant and equal to its initial value ω_p. The angular velocity ω_p is merely exchanged between the 1- and 2-axes at a changing rate as the spin rate changes. This exchange rate can be employed to measure the spin rate, as described later.

Motion Relative to Space Coordinates

The motion of the vehicle relative to the space-fixed x-, y-, and z-axes is described by Lagrange's equations of motion (Ref. 3). The motion is described in terms of Euler's angles, which are illustrated in Fig. 8. The plane containing the 1- and 2-axes intersects the plane containing the x- and y-axes along a line called the "line of nodes." The angle between the x-axis and the line of nodes is ϕ, and the angle between the line of nodes and the 1-axis is ψ. The angle between the z-axis and the 3-axis is θ, the "precession angle." From geometry it can be shown (Ref. 3) that ϕ, ψ, and θ are related to the spin rate ω_3 by

$$\dot{\psi} + \dot{\phi} \cos \theta = \omega_3 \tag{16}$$

The angular velocity of the line of nodes, $\dot{\phi}$, is the "precession rate."

With a torque of DF about the 3-axis and zero about the 1- and 2-axes, Lagrange's equation for the rate of change of the precession angle θ is

$$\ddot{\theta} = \phi \sin\theta \left(\dot{\phi} \cos \theta - \frac{I_3}{I_1} \omega_3 \right) \tag{17}$$

For the small angular accelerations obtained in an ion-motor test, $\ddot{\theta}$ is very small compared with the quantities on the right side of Eq. 17. To a close approximation, Eq. 17 reduces to

$$\dot{\phi} = \frac{I_3 \omega_3}{I_1 \cos \theta} \tag{18}$$

Substituting this expression for $\dot{\phi}$ into Eq. 16 yields the following expression for the spin rate $\dot{\psi}$ relative to the line of nodes:

$$\dot{\psi} = \left(1 - \frac{I_3}{I_1} \right) \omega_3 \tag{19}$$

Fig. 9 shows the relationship between the angular momentum $I_3 \omega_3$ about the spin axis, the angular momentum $I_1 \omega_p$ perpendicular to the spin axis, the total angular momentum L, and the precession angle θ. The total angular momentum is equal to the vector sum of $I_3 \omega_3$ and $I_1 \omega_p$. Thus,

$$L^2 = I_3^2 \omega_3^2 + I_1^2 \omega_p^2 \tag{20}$$

At the small angular accelerations of interest, the total angular-momentum vector almost coincides with the z-axis. Hence, the precession angle θ is given, to a close approximation, by

$$\tan \theta = \frac{I_1 \omega_p}{I_3 \omega_3} \tag{21}$$

With I_1, I_3, F, D, ω_0, and ω_p given, Eq. 14, 18, 19 and 21 constitute a complete description of the motion of the ion-motor test-vehicle relative to the space-fixed x-, y-, and z-axes. Except for Eq. 14, these equations are the same as those for a free body with no applied torque.

Fig. 10 shows the motion, during a 1.4-hr test, of the vehicle shown in Fig. 6, for which $F = 0.010$ lb_f, $D = 5.5$ in., $I_1 = 56.6$ lb_f in. sec^2, $I_3 = 11.1$ lb_f in. sec^2, and $\omega_0 = 160$ rpm. The spin rate ω_3, the precession rate $\dot{\phi}$, and the precession angle θ are shown as a function of time for an initial precession angle of 2.0 deg ($\omega_p = 1.1$ rpm), an easily attained alignment.

It is seen that the spin rate ω_3 changes linearly with time, decreasing to zero at 57 min and reaching -75 rpm at 84 min, the end of the test.

The precession rate $\dot{\phi}$ starts at 31 rpm, reaches a minimum of 1.1 rpm (equal to ω_p) at 57 min, and increases again to 15 rpm at 84 min. The precession angle θ changes slowly at first, reaching 10 deg at 46 min. The vehicle then rapidly reverses direction, θ reaching 170 deg at 68 min and increasing slowly thereafter.

The motion shown in Fig. 10 is strictly correct only when the moments of inertia I_1 and I_2 are exactly equal and there are no torques about the 1- and 2-axes, conditions which will not be completely met in practice. With a 1% difference between I_1 and I_2, for example, the angular acceleration $\dot{\omega}_3$ will not be constant at 2.8 rpm/min but will oscillate about this value by about ± 7% at a frequency varying from 4.3 cps at the start of the test to 2.1 cps as the spin rate goes through zero. Thus, in practice, there will be small oscillations about the average motion shown in Fig. 10, and for maximum accuracy in determining the thrust these oscillations must be taken into account in reducing the spin-rate data.

Effect of Extraneous Torques

There are two sources of extraneous torques which can alter the spin rate and hence lead to errors in determining the thrust of the ion motor. These are (1) torques due to the Earth's magnetic field and (2) spin rate damping due to structural deflections and consequent energy dissipation in the vehicle.

Torque Due to the Earth's Magnetic Field

The Earth's magnetic field induces eddy currents in the conducting shell of a spinning vehicle, causing the spin rate to decrease. Smythe (Ref. 4) shows that the torque on a

spinning cylindrical shell in a uniform magnetic field perpendicular to the axis of the cylinder is

$$T = \frac{4\pi R h a^3 B^2 L \omega}{4R^2 + \omega^2 \mu_v^2 a^2 h^2} \tag{22}$$

where ω is the spin rate, R is the resistivity of the shell, h is the thickness of the shell, a is the radius of the cylinder, B is the magnetic field, L is the length of the cylinder, and μ_v is the permeability of a vacuum. Representing the vehicle of Fig. 6 by an aluminum cylinder of 14-in. diameter, 12-in. length (the total length of the battery, inverter, and telemetry containers), and 0.063-in. wall thickness, the torque given by Eq. 22 for a spin rate of ω = 160 rpm and B = 0.3 gauss (the Earth's magnetic field) is 4×10^{-5} lb_f in. This is less than 0.1% of the ion-motor torque and is therefore not a significant source of error.

The second term in the denominator of Eq. 22 is much smaller than the first. Hence, the magnetically induced torque is proportional to the spin rate ω and becomes even more negligible as the spin rate decreases.

Torque Due to Non-Rigidity of Vehicle

The ion-motor test vehicle is not perfectly rigid but has parts which deflect and produce small torques which, if appreciable and not corrected for, lead to errors in the thrust measurement. The rate of change of the spin rate ω_3 due to these deflections must therefore be considered. In the treatment that follows it will be assumed that the effect of the deflections is small enough that the rigid-body equations derived previously can be employed to describe the gross motion.

The kinetic energy of rotation about the 3-axis of the vehicle is $I_3 \omega_3^2/2$ and that perpendicular to the 3-axis is $I_1 \omega_p^2/2$. Hence, the total kinetic energy of rotation is

$$E = \frac{I_3 \omega_3^2}{2} + \frac{I_1 \omega_p^2}{2} \tag{23}$$

Employing Eq. 20 the energy can be written

$$E = \frac{L^2}{2 I_1} + \frac{I_3 \omega_3^2}{2}\left(1 - \frac{I_3}{I_1}\right) \tag{24}$$

Because of vehicle deflection the energy can change in the absence of ion-motor thrust; that is, with the angular momentum L constant. From Eq. 24 this rate of change is

$$\frac{dE}{dt} = I_3\omega_3 \left(1 - \frac{I_3}{I_1}\right)\frac{d\omega_3}{dt} \tag{25}$$

Rearranging gives the angular acceleration due to structural deflections and consequent energy dissipation. This acceleration is

$$\frac{d\omega_3}{dt} = \frac{\frac{dE}{dt}}{I_3\omega_3\left(1 - \frac{I_3}{I_1}\right)} \tag{26}$$

Since dE/dt is inherently negative, Eq. 26 shows that for a vehicle like that of Fig. 6, for which $I_1 > I_3$, the energy dissipation acts to decrease the magnitude of the spin rate. The ion motor is aided when the spin is decreasing and opposed when the spin is increasing. This suggests the possibility of cancelling out the energy-dissipation error by averaging thrusts measured before and after the spin rate goes through zero.

Ref. 5 shows that when I_1 is substantially larger than I_3 the chief force causing energy dissipation is the time-varying coriolis force given by

$$F_c = 2\Delta m\, \dot{\psi}\, \dot{\phi}\, r \sin\theta \cos(\dot{\psi} t) \tag{27}$$

where F_c is the instantaneous coriolis force acting on an element of mass Δm located at distance r from the 3-axis. The force acts parallel to the 3-axis.

Eq. 27 shows that the change in the coriolis force on Δm during one-half revolution of the vehicle relative to the line of nodes is

$$\Delta F_c = 4\Delta m\, \dot{\psi}\, \dot{\phi}\, r \sin\theta \tag{28}$$

The change in force ΔF_c produces a deflection of Δm equal to that which would be produced by subjecting Δm to an acceleration

of $\Delta F_c / \Delta m$ g's. If the deflection of Δm is k units per g of acceleration, the deflection Δx can be written

$$\Delta x = k \frac{\Delta F_c}{\Delta m} \tag{29}$$

The work Δw done on Δm is equal to the average force times the deflection. Thus,

$$\begin{aligned} \Delta w &= \frac{\Delta F_c \ \Delta x}{2} \\ &= \frac{k \ \Delta F_c^{\,2}}{2 \Delta m} \end{aligned} \tag{30}$$

If a fraction γ of this work is dissipated as heat, the energy dissipated by Δm during one-half revolution of the vehicle relative to the line of nodes is

$$\Delta E = \frac{\gamma k \ \Delta F_c^{\,2}}{2 \Delta m} \tag{31}$$

and the energy dissipated by Δm per unit time is

$$\Delta E \frac{\dot{\psi}}{\pi} = \frac{\gamma k \ \Delta F_c^{\,2} \dot{\psi}}{2 \pi \Delta m} \tag{32}$$

Substituting ΔF_c from Eq. 28 and integrating over the vehicle yields the following relation for the energy dissipation rate:

$$\frac{dE}{dt} = \frac{8}{\pi} \ \dot{\psi}^3 \ \dot{\phi}^2 \sin^2 \theta \int_M \gamma k \, r^2 \, dm \tag{33}$$

The quantities $\dot{\psi}$ and $\dot{\phi}$ can be written in terms of the spin rate ω_3 and the precession angle θ by means of Eq. 18 and 19, yielding

$$\frac{dE}{dt} = -\frac{8}{\pi} \left(1 - \frac{I_3}{I_1}\right)^3 \left(\frac{I_3}{I_1}\right)^2 \omega_3^{\,5} \tan^2 \theta \int_M \gamma k \, r^2 \, dm \tag{34}$$

Substituting the rate of energy dissipation from Eq. 34 into Eq. 26 gives the desired relation for the angular acceleration due to structural deflections. Thus,

$$\frac{d\omega_3}{dt} = -\lambda\left[\left(1 - \frac{I_3}{I_1}\right)\left(\frac{I_3}{I_1}\right)\omega_3^2 \tan\theta\right]^2 \qquad (35)$$

where

$$\lambda = \frac{8}{\pi I_3}\int_M \gamma k\, r^2\, dm$$

Eq. 35 shows that for a given vehicle flexibility, as expressed by the integral λ, the angular acceleration due to energy dissipation is proportional to the square of the moment of inertia ratio I_3/I_1 and to the fourth power of the spin rate ω_3. Thus, a long, slender vehicle is desirable for minimizing this source of error.

Evaluation of the integral λ requires detailed knowledge of the vehicle structure. To get an idea of its possible magnitude, the value of λ was calculated for the Explorer III satellite, using data from Ref. 5. Explorer III was launched with a spin rate of 600 rpm and a precession angle of about 7 deg. Its moment-of-inertia ratio was $I_1/I_3 = 82$, and the initial angular acceleration due to energy dissipation was observed to be $d\omega_3/dt = -0.004$ rpm/min. Substituting these quantities in Eq. 35 yields $\lambda = 2 \times 10^{-7}$ sec^2.

If the ion-motor test vehicle of Fig. 6 were built with the same degree of rigidity as Explorer III, it would have a roughly similar value of λ. The corresponding angular deceleration of the ion-motor vehicle for an initial precession angle of 2.0 deg is 3×10^{-4} rpm/min and decreases as the vehicle despins. Even if the initial precession angle were 10 deg, the initial (and maximum) angular deceleration due to energy dissipation would be only 7×10^{-3} rpm/min. These decelerations are only 0.01% and 0.25%, respectively, of the deceleration produced by the ion motor. Thus, if the ion-motor test vehicle can be made reasonably rigid and the initial precession angle kept small, the error in thrust measurement due to energy dissipation will be negligible.

SPIN-RATE MEASUREMENT TECHNIQUES

Spin-Rate Counting with Accelerometer, Inertia Switch, or Rate Gyro

Referring to Fig. 7, suppose that an accelerometer is mounted on the 3-axis at a distance s from the center of mass, with its sensitive direction parallel to the 2-axis. The acceleration it reads is

$$a = s \frac{d\omega_1}{dt} \tag{36}$$

Differentiating Eq. 12 to obtain the angular acceleration around the 1-axis and substituting in Eq. 36 yields

$$a = s\omega_p\omega_3 \left(1 - \frac{I_3}{I_1}\right) \cos\left[\frac{1}{2}\left(1 - \frac{I_3}{I_1}\right)(\omega_3 + \omega_0)\, t + \text{const}\right] \tag{37}$$

Thus, the frequency of the accelerometer output is

$$f = \frac{1}{4\pi} \left(1 - \frac{I_3}{I_1}\right)(\omega_3 + \omega_0) \tag{38}$$

Hence, the spin rate ω_3 can be determined from the telemetered accelerometer frequency. The accelerometer need not be calibrated; in fact, an inertia switch could be employed instead. A rate gyro mounted on the 1- or 2-axis would also show an output variation at the frequency given by Eq. 38.

The amplitude of the acceleration seen by the accelerometer or inertia switch is

$$a = s\omega_p\omega_3 \left(1 - \frac{I_3}{I_1}\right) \tag{39}$$

Thus, there is insufficient acceleration to operate the accelerometer or inertia switch while the spin rate goes through zero. For the vehicle shown in Fig. 6, however, the acceleration amplitude at the top of the inverter and telemetry box ($s = 17.5$ in.) is greater than 10^{-3} g's, a measurable amplitude, for all but 2 min of the test.

Sun-Sensor and Signal-Strength Measurements

The spin rate can also be measured by observing the telemetered frequency of Sun or Earth sensors in the vehicle, and by observing the frequency of signal-strength variations on the ground. The latter technique is illustrated in Fig. 11, which shows a portion of the signal-strength record from Explorer I shortly after launching. Even though the Explorer I antenna was not specifically designed to give clear-cut signal-strength variations, it can be seen that the number of cycles of signal strength in a given time can be determined to within about 0.2 cycles.

Unfortunately, the frequency of signal-strength, or Sun-sensor output, variations is not exactly the same as the spin rate ω_3 when the vehicle is precessing. To see how these frequencies are related to ω_3 consider the motion of the vehicle at some time during the test, as shown in Fig. 12. The z-axis is the axis of symmetry of the vehicle's rotation, and the orientation of the vehicle relative to the x-, y-, and z-axes is described by the Euler angles θ, ϕ, and ψ as before. A "reference line" to the Sun or to the ground receiving station is drawn at angle α from the z-axis, with its projection on the x–y plane at an angle β from the x-axis. A "reference plane" is drawn through the reference line and the 3-axis, intersecting the x–y plane at angle A from the x-axis. It can be shown from geometry that angle A is given by

$$\frac{\sqrt{\left[\frac{\tan(A-\beta)}{\sin\alpha\cos\alpha}\right]^2+\cot^2\alpha}\ \sin\left[\tan^{-1}\left(\frac{\tan[A-\beta]}{\cos^2\alpha}\right)+\beta-A\right]}{\cos(\phi-A)}=\tan\theta \tag{40}$$

Suppose that the antenna is mounted so that there is a peak (or a null) in the antenna pattern in the 1–3 plane. Suppose, also, that the vehicle has a Sun sensor which sees the Sun when the Sun is in the 1–3 plane. The intersection of the 1–3 plane with the x–y plane occurs at angle B, which, from geometry, is given by

$$\tan(B-\phi)=\frac{\tan\psi}{\cos\theta} \tag{41}$$

The peak (or null) in signal strength, or the peak in Sun-sensor output, occurs when the 1–3 plane coincides with the reference plane; that is, when A = B.

As an example, consider the motion of the vehicle shown in Fig. 6 at a time 54 min after the start of the test. The spin rate at that time is $\omega_3 = 10.0$ rpm, the precession rate is $\dot{\phi} = 2.24$ rpm, and the precession angle is $\theta = 29$ deg. From Eq. 19 the spin rate relative to the line of nodes is 8.04 rpm. Fig. 12 shows angle B, the angle to the intersection of the 1–3 and x–y planes, as a function of time, assuming $\phi = \psi = 0$ at $t = 0$. Angle B increases linearly with time (with a slight undulation, not shown) at 10.23 rpm, the sum of $\dot{\phi}$ and $\dot{\psi}$.

Suppose that the reference line to the Sun or the ground receiving station is at $\alpha = 45$ deg and $\beta = 0$. Suppose also that $\dot{\alpha} = \dot{\beta} = 0$, as would be the case, to a close approximation, for a line drawn to the Sun. Fig. 13 shows angle A, the angle to the intersection of the reference plane and x–y plane, as a function of time for these conditions. It is seen that angle A oscillates between +35 deg and -35 deg. The frequency of oscillation is 2.24 cps, equal to $\dot{\phi}$, but the variation of A is not sinusoidal.

The reference plane and the 1–3 plane coincide (A = B) at irregular intervals. The four coincidences shown in Fig. 13 occur at 0.5, 6.0, and 11.1, and 17.3 sec. Thus, the period between the first and second peaks in signal strength or in Sun-sensor output is 5.5 sec, between the second and third 5.1 sec, and between the third and fourth 6.2 sec. These periods correspond to frequencies of 10.9, 11.8, and 9.7 rpm, respectively, whereas ω_3 is 10.0 rpm. Thus, the spin rate ω_3 can only be determined within about 15% from measurement of the time between one successive pair of Sun-sensor or signal-strength peaks, for the assumed conditions. The accuracy improves when the periods between many successive peaks are averaged together, but for the conditions of Fig. 13 the averaging would have to cover several minutes.

Early in the test, when the precession angle is small, the coincidences of angles A and B occur at more regular intervals and ω_3 can be equated, with good accuracy, to the Sun-sensor or signal-strength frequency. At other times, accurate determination of the spin rate ω_3 requires knowledge of the vehicle precession angle so that Eq. 40 and 41 can be fitted to the data to determine ω_3. In addition, for signal-strength measurements, the motion of the vehicle relative to the receiving station produces changes in the reference-line angles α and β, which must also be determined and substituted into Eq. 40.

CONCLUSIONS

1. Tests of ion rocket motors in space at useful thrust levels and durations are possible using battery power supplies and available launching vehicles.

2. The relatively inexpensive Scout vehicle is adequate for simple ion motor tests. The Scout can launch an ion motor of 10-mlb thrust with its power supply and telemetry equipment for a test duration of about 1.4 hr.

3. The thrust of the ion motor can be determined from changes in the vehicle flight path, motion of the vehicle relative to a reference object, or angular acceleration of the vehicle. The latter appears to be the simplest and most accurate.

4. For an angular-acceleration experiment the moment of inertia about the spin axis should be smaller than the moments of inertia perpendicular to the spin axis to maximize the angular acceleration and minimize errors due to non-rigidity of the vehicle. The two moments of inertia perpendicular to the spin axis should be equal to provide a steady angular acceleration which is a function of thrust only.

5. Errors in thrust measurement due to the Earth's magnetic field are negligible. Errors due to non-rigidity of the vehicle can be made negligible by good structural design.

6. The spin rate can be measured by an accelerometer, inertia switch, or rate gyro within the vehicle. These give an output varying at a frequency related to the spin frequency and independent of precession angle and vehicle orientation. The spin rate can also be obtained from Sun-sensor and signal-strength measurements which give the spin rate relative to the Sun or to the ground receiving station, but these require knowledge of the vehicle's orientation and precession angle.

NOMENCLATURE

a	accelerometer acceleration
$\mathcal{a}$	acceleration amplitude
A	angle from x-axis to intersection of x–y and reference planes
B	angle from x-axis to intersection of x–y and 1–3 planes
c	exhaust velocity
D	distance from center of mass of vehicle to thrust line of ion motor
E	kinetic energy of rotation
f	acceleration frequency
F	ion-motor thrust
F_c	coriolis force
F_e	electrostatic attraction between vehicle and exhaust
I_1, I_2, I_3	moments of inertia about 1-, 2-, and 3-axes
k	structural deflection per g of acceleration
L	total angular momentum
$\dot{m}$	propellant flow rate
M	vehicle mass
M_b	battery mass
M_m	ion-motor mass
P_b	battery output power
P_{bi}	portion of battery power supplied to inverter
P_i	inverter output power

P_m	ion-motor input power
P_t	telemetry input power
r	radius to mass element
s	distance from center of mass to accelerometer
t	time
T	torque
v	vehicle velocity
α	angle from z-axis to reference line
β	angle from x-axis to projection of reference line on x–y plane
γ	fraction of deflection work dissipated as heat
Δm	element of vehicle mass
Δw	work done by coriolis force
Δx	structural deflection
θ	angle from z-axis to 3-axis
ϕ	angle from x-axis to line of nodes
ψ	angle from line of nodes to 1-axis
$\omega_1, \omega_2, \omega_3$	angular velocities around the 1-, 2-, and 3-axes
ω_0	initial angular velocity around the 3-axis
ω_p	initial angular velocity perpendicular to the 3-axis

REFERENCES

1. Schult, R. W., and Stafford, W. T., The State of Development of Silver Oxide-Zinc and Nickel-Cadium Batteries, Report No. STL/TR-60-0000-09034, Space Technology Laboratories, Inc., Los Angeles, California, February, 1960

2. Scout Manual, Appendix D, National Aeronautics and Space Administration, Langley Field, Virginia, September 19, 1960

3. Slater, John C., and Frank, Nathaniel H., Mechanics, McGraw-Hill Book Company, Inc., New York, 1947

4. Smythe, William R., Static and Dynamic Electricity, McGraw-Hill Book Company, Inc., New York, 1950

5. Pilkington, William C., and Wells, Willard W., "Vehicle Motions as Inferred from Radio-Signal-Strength Records," Avionics Research: Satellites and Problems of Long Range Detection and Tracking, Pergamon Press, New York, 1960

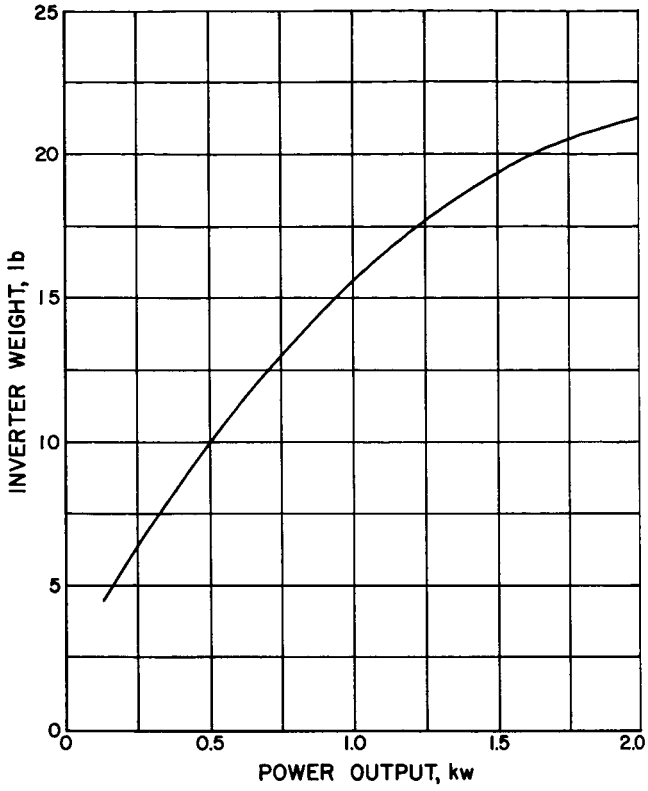

Fig. 1. Approximate inverter weight as a function of output power.

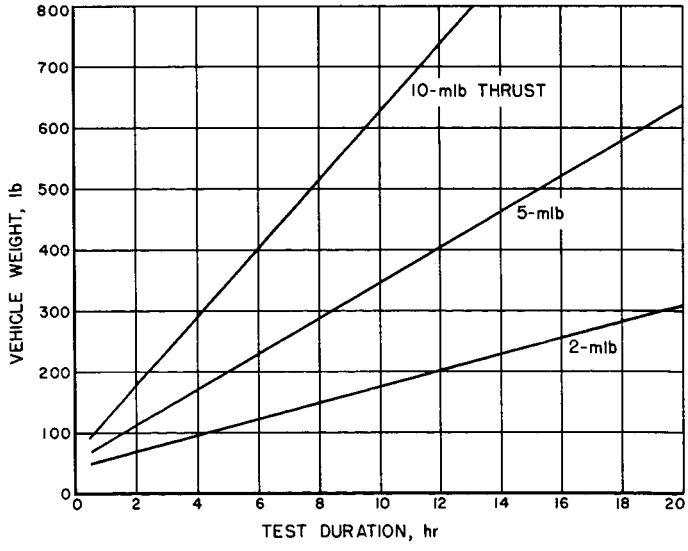

Fig. 2. Weight of ion-motor test vehicle as a function of thrust and test duration.

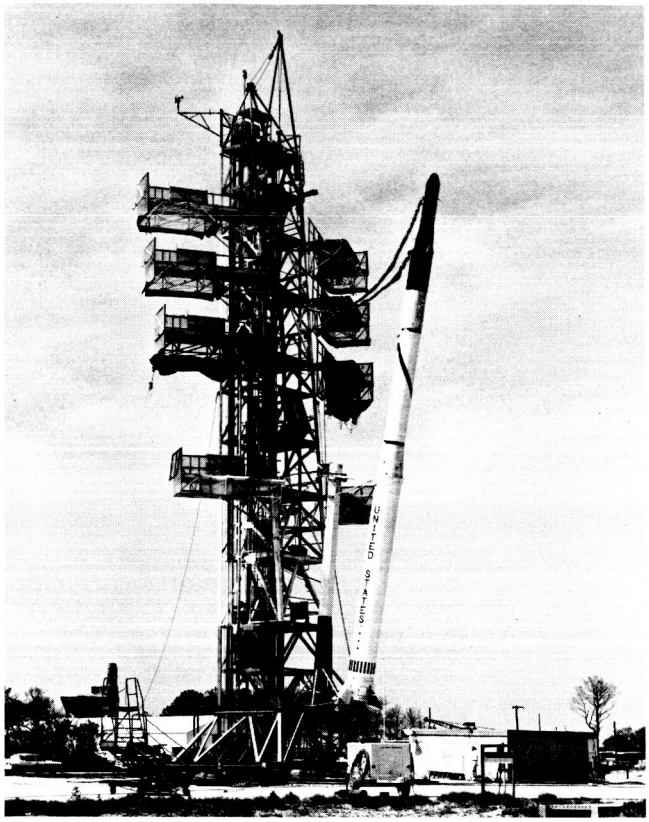

Fig. 3. Scout research vehicle.

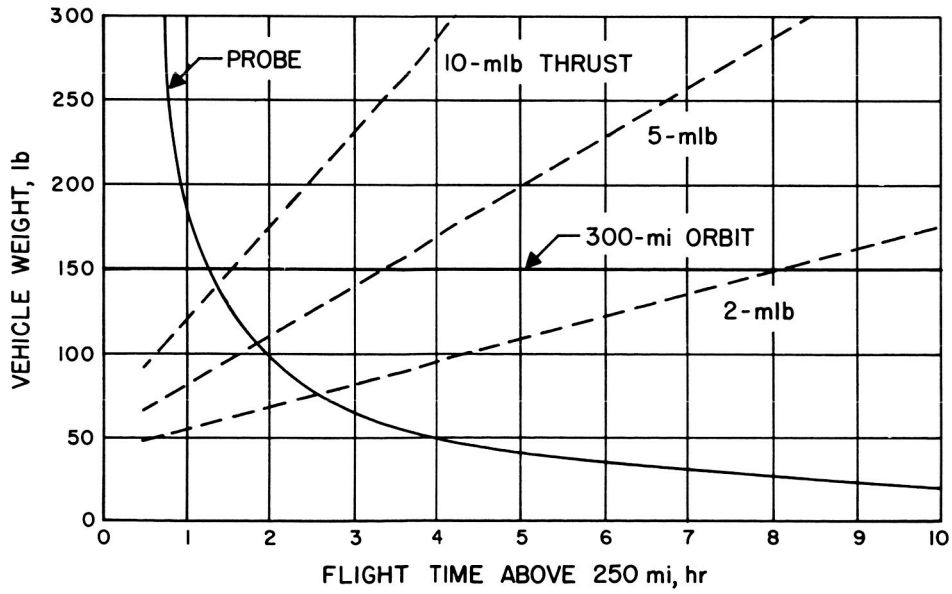

Fig. 4. Capability of Scout for launching ion-motor test vehicles.

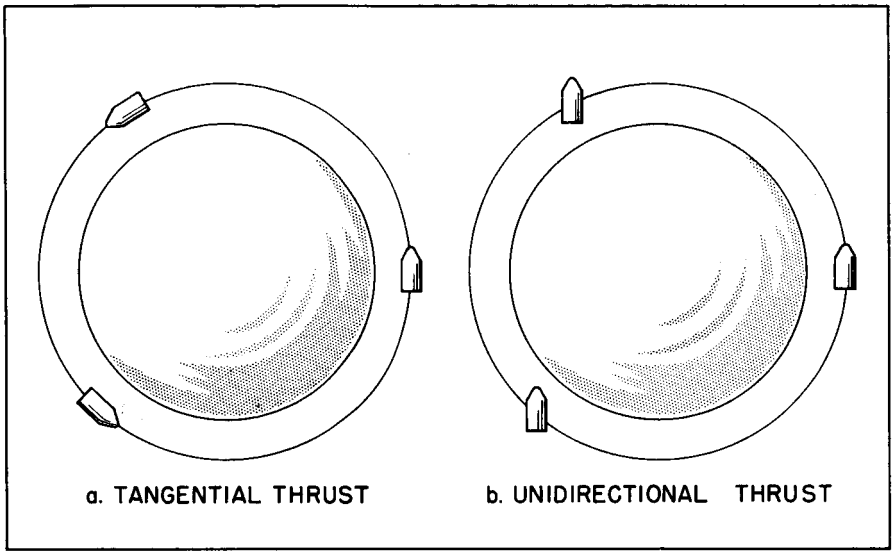

Fig. 5. Thrust programs for thrust measurement by orbital changes.

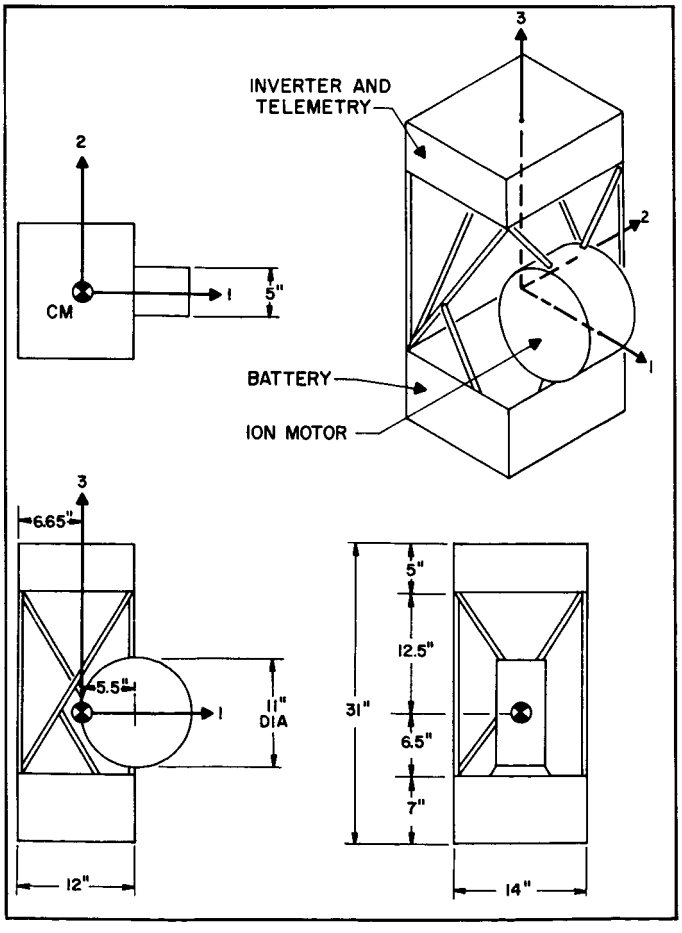

Fig. 6. Test-vehicle configuration for 10-mlb ion-motor launched by Scout.

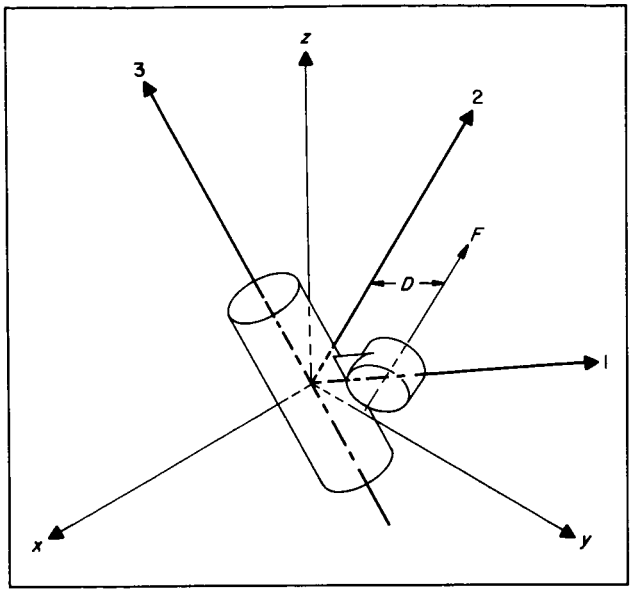

Fig. 7. Axes for describing motion of ion-motor test vehicle.

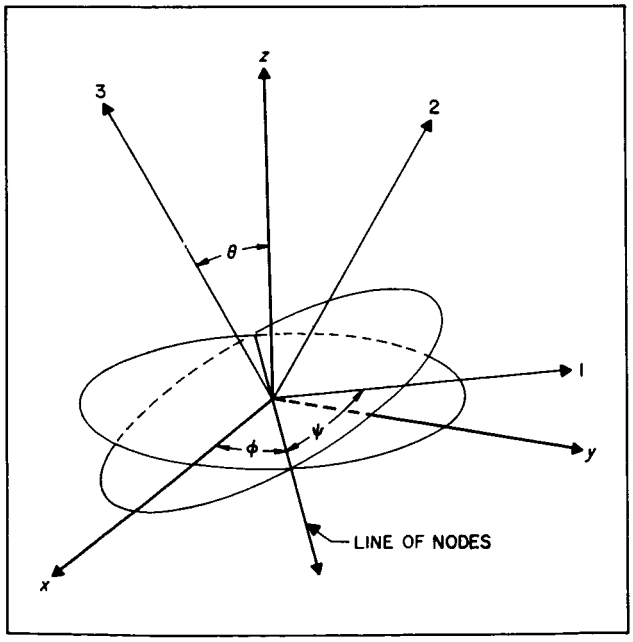

Fig. 8. Orientation of ion-motor test vehicle in Euler's angles.

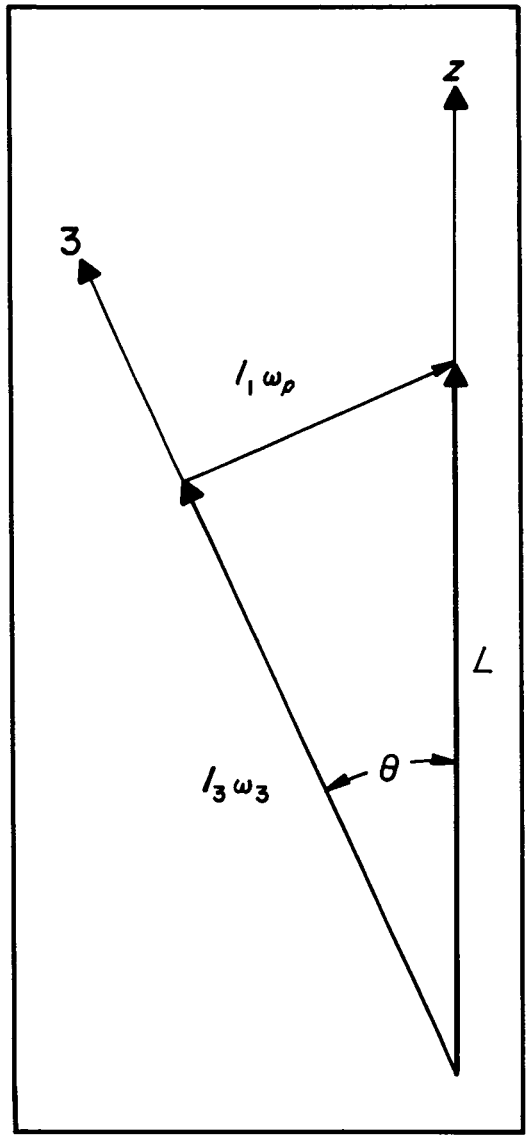

Fig. 9. Relation between angular momentum and precession angle.

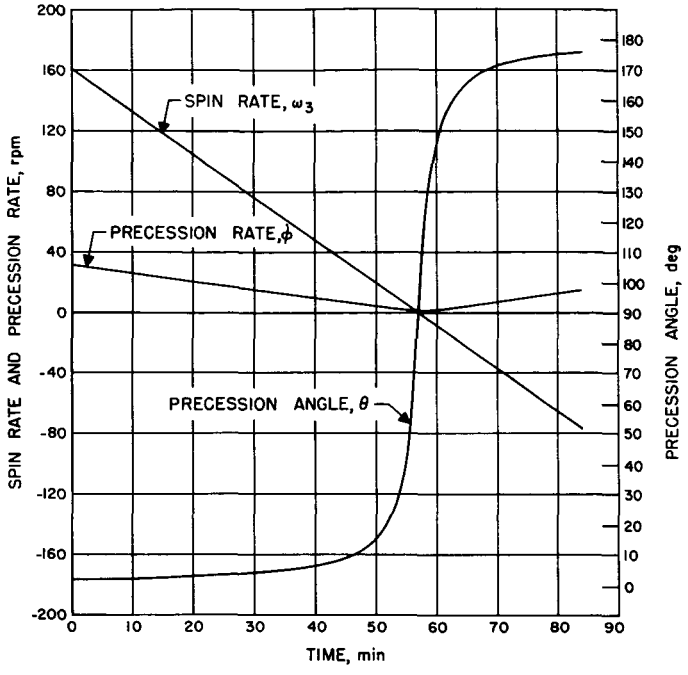

Fig. 10. Motion of ion-motor test vehicle as a function of time.

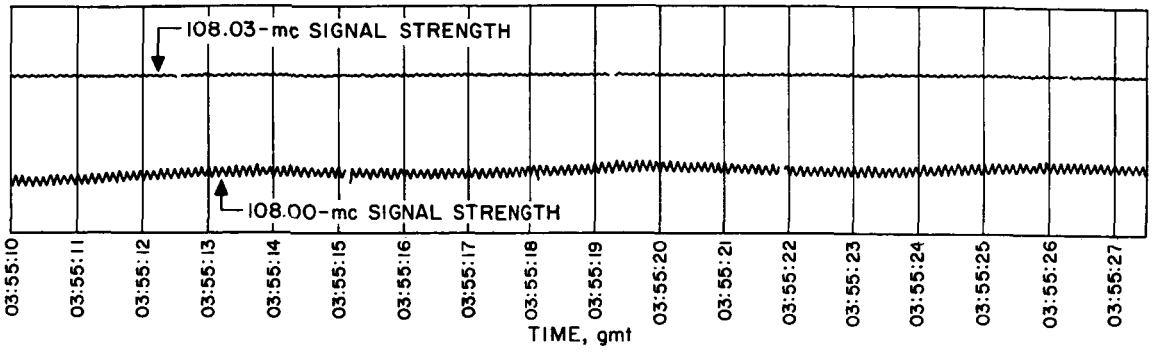

Fig. 11. Reproduction of a portion of the signal-strength record of Explorer I

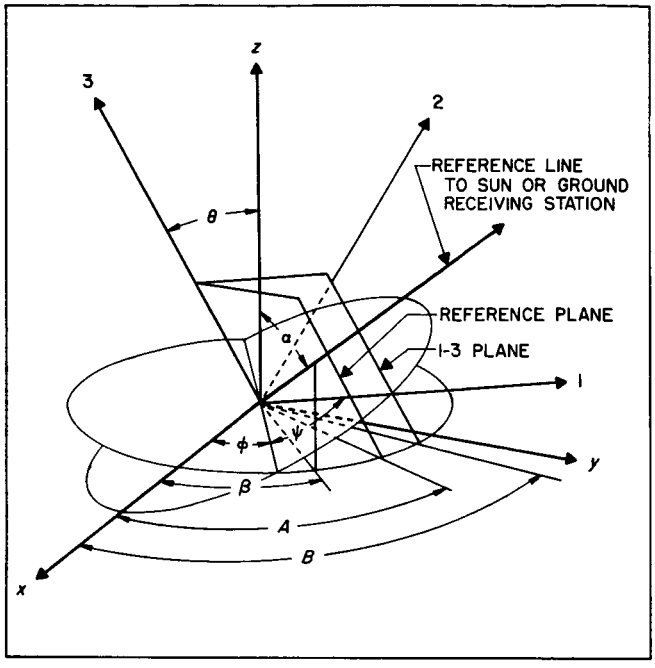

Fig. 12. Orientation of ion-motor test vehicle relative to Sun or ground receiving station.

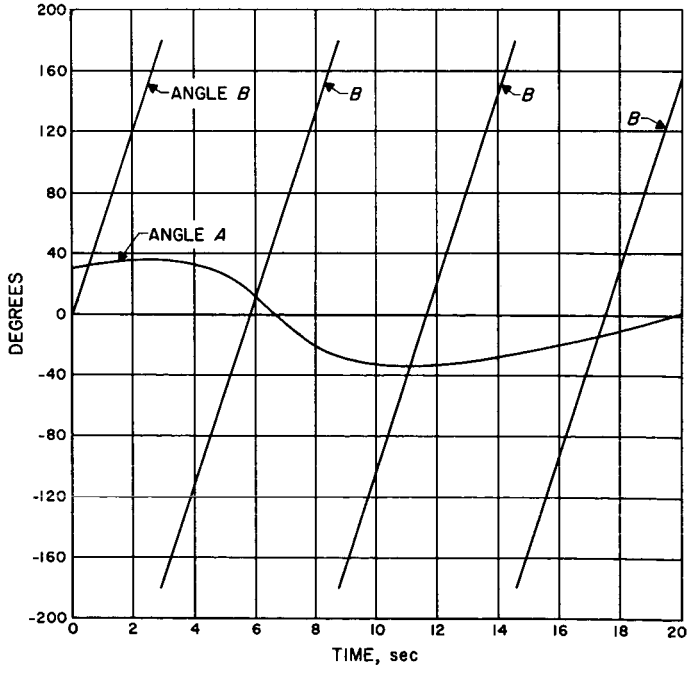

Fig. 13. Angle to reference plane, A, and angle to 1–3 plane, B, as a function of time.